

## **Color Imaging of Shock Front Emergence in TNT**

**by Kevin McNesby, Gerrit Sutherland, and Richard Benjamin**

**ARL-TR-6181**

**October 2012**

## **NOTICES**

### **Disclaimers**

The findings in this report are not to be construed as an official Department of the Army position unless so designated by other authorized documents.

Citation of manufacturer's or trade names does not constitute an official endorsement or approval of the use thereof.

Destroy this report when it is no longer needed. Do not return it to the originator.

# **Army Research Laboratory**

Aberdeen Proving Ground, MD 21005-5066

---

---

**ARL-TR-6181**

**October 2012**

---

---

## **Color Imaging of Shock Front Emergence in TNT**

**Kevin McNesby, Gerrit Sutherland, and Richard Benjamin**  
**Weapons and Material Research Directorate, ARL**

REPORT DOCUMENTATION PAGE			Form Approved OMB No. 0704-0188		
Public reporting burden for this collection of information is estimated to average 1 hour per response, including the time for reviewing instructions, searching existing data sources, gathering and maintaining the data needed, and completing and reviewing the collection information. Send comments regarding this burden estimate or any other aspect of this collection of information, including suggestions for reducing the burden, to Department of Defense, Washington Headquarters Services, Directorate for Information Operations and Reports (0704-0188), 1215 Jefferson Davis Highway, Suite 1204, Arlington, VA 22202-4302. Respondents should be aware that notwithstanding any other provision of law, no person shall be subject to any penalty for failing to comply with a collection of information if it does not display a currently valid OMB control number. <b>PLEASE DO NOT RETURN YOUR FORM TO THE ABOVE ADDRESS.</b>					
1. REPORT DATE (DD-MM-YYYY) October 2012		2. REPORT TYPE Final		3. DATES COVERED (From - To) 10 January 2010 to 6 March 2012	
4. TITLE AND SUBTITLE Color Imaging of Shock Front Emergence in TNT			5a. CONTRACT NUMBER		
			5b. GRANT NUMBER		
			5c. PROGRAM ELEMENT NUMBER		
6. AUTHOR(S) Kevin McNesby, Gerrit Sutherland, and Richard Benjamin			5d. PROJECT NUMBER		
			5e. TASK NUMBER		
			5f. WORK UNIT NUMBER		
7. PERFORMING ORGANIZATION NAME(S) AND ADDRESS(ES) U.S. Army Research Laboratory ATTN: RDRL-WML-C Aberdeen Proving Ground, MD 21005-5066			8. PERFORMING ORGANIZATION REPORT NUMBER ARL-TR-6181		
9. SPONSORING/MONITORING AGENCY NAME(S) AND ADDRESS(ES)			10. SPONSOR/MONITOR'S ACRONYM(S)		
			11. SPONSOR/MONITOR'S REPORT NUMBER(S)		
12. DISTRIBUTION/AVAILABILITY STATEMENT Approved for public release; distribution unlimited.					
13. SUPPLEMENTARY NOTES					
14. ABSTRACT This report describes the use of high speed color digital optical imaging of light emission at the shock/detonation front to determine the planarity (or lack thereof) of a detonation wave produced in an explosive sample using a 4-inch diameter plane wave generator (lens). A high speed, color digital framing camera (Cordin Company Model 570) was used to record images of detonation front emergence from samples of the solid high explosive TNT (trinitrotoluene, C <sub>7</sub> H <sub>5</sub> N <sub>3</sub> O <sub>6</sub> ). Frame-by-frame images of the event are deconstructed into red, green, and blue matrices used by the digital camera system to produce color images. CTH-based calculations (CTH-based calculations (a hydrodynamic computer code developed at Sandia National Laboratories), predicting the spatial profile of the shock/detonation front as it emerges from the solid explosive surface, are compared with bandwidth-specific contour maps made using the color matrices. The correlation between contour maps of light emission at different bandwidths and predicted shock/detonation profiles is discussed.					
15. SUBJECT TERMS Explosives, detonation imaging, digital color imaging					
16. SECURITY CLASSIFICATION OF:			17. LIMITATION OF ABSTRACT	18. NUMBER OF PAGES	19a. NAME OF RESPONSIBLE PERSON
a. REPORT	b. ABSTRACT	c. THIS PAGE			Kevin L. McNesby
Unclassified	Unclassified	Unclassified	SAR	20	19b. TELEPHONE NUMBER (Include area code) (410) 306-1383

---

## Contents

---

<b>List of Figures</b>	<b>iv</b>
<b>1. Introduction</b>	<b>1</b>
<b>2. Experimental</b>	<b>2</b>
<b>3. Digital Color Imaging</b>	<b>3</b>
<b>4. Results</b>	<b>5</b>
<b>5. Discussion</b>	<b>8</b>
<b>6. Conclusions</b>	<b>11</b>
<b>7. References</b>	<b>12</b>
<b>Distribution List</b>	<b>13</b>

---

## List of Figures

---

Figure 1. A plane wave generator of the type manufactured at the ARL. ....	1
Figure 2. ARL explosive PWG with TNT test material. ....	2
Figure 3. The Cordin Company Model 570 digital color framing camera. ....	3
Figure 4. a. A schematic of the Bayer-type mask; b. A calibration spectrograph for the Bayer-type mask; and c. A schematic of deconvolution of a raw color image. ....	4
Figure 5. a. A color image of a dispersed, reflected He:Ne laser near a wavelength of 635 nm; b. The red matrix corresponding to a. c. The green matrix corresponding to a. (note some response) and d. The blue matrix corresponding to a. ....	4
Figure 6. A series of images of light emission from the face of the PWG following initiation. The frame denoted as $t_0$ corresponds to arrival of the shock wave at the PWG face. R,G,B refer to pixel color matrices (red, green, blue) used by the camera to produce color images. ....	5
Figure 7. Contour maps of red matrices up to the time of the shock wave emerging from the face of the PWG. ....	6
Figure 8. Cross sectional contour maps of the three color matrices. ....	7
Figure 9: Side view of a contour map of red matrix cross sections near the time when the shock wave emerges from the face of the PWL. ....	8
Figure 10. A series of 2-dimensional graphs of single cross sections through the red matrices viewed perpendicular to the long axis of the glass cover slide. ....	9
Figure 11. CTH simulations of shock wave transit in the ARL PWG. ....	10

---

## 1. Introduction

---

One-dimensionality of basic shock relations motivates scientists and engineers to design experiments using planar shocks (1). However, single point initiation of chemical reactions proceeding at detonation velocity in an explosive material usually produces an outward radiating spherical shock wave. Attempts to produce planar shock waves typically rely on flyer plates to initiate chemistry, or employ contoured and layered explosive mixtures in which detonation velocities of different components are used to achieve a shock wave profile at a given distance from the point of initiation (2).

Planar shock waves achieved by the latter method use a device that is referred to as an explosive plane wave generator (PWG), or plane wave lens (PWL). The plane wave generator appears as two concentric cones of explosive material. The inner cone material exhibits a slower detonation velocity than the outer cone material (3). A cross section of the plane wave generator manufactured at the U.S. Army Research Laboratory (ARL) is shown in figure 1.

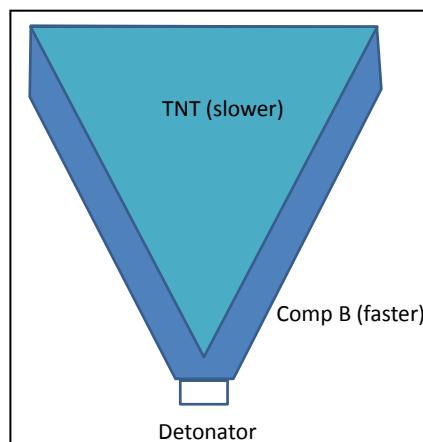


Figure 1. A plane wave generator of the type manufactured at the ARL.

The angle of the cone is chosen so that the vertical component of the detonation velocity in the outer cone explosive is equal to the detonation velocity of the inner cone explosive. The detonation wave moving in the outer cone/higher velocity explosive continuously initiates detonation in the inner cone/low velocity explosive at the interface, such that the detonation front remains planar as it proceeds away from the point of initiation (3).

Determination of the planarity of the shock wave as it emerges from the PWG is usually accomplished using piezo pins to measure displacement of the free surface of the PWG, or measured optically using shock-induced light emission from a confined gas at the PWG surface (2).

In the work described here, we record digital color images of light emitted by the explosive as the detonation proceeds within the material. Each color component of the digital image is analyzed to determine if the detonation front within the solid explosive can be measured prior to emergence. We investigate the use of digital signal processing techniques to evaluate the planarity of the shock wave within the interior of the explosive and as it emerges from the explosive. Results using these techniques are compared to simulations using the CTH hydrodynamic computer code (4).

---

## 2. Experimental

---

The PWG used here was manufactured by the Energetics Technology Branch of the Weapons and Materials Research Directorate of the ARL. The inner cone consisted of milspec trinitrotoluene ( $C_7H_5N_3O_6$ , detonation velocity 6.9 mm/microsecond). The outer cone consisted of milspec Composition B (60:40 RDX (trimethylene trinitramine,  $C_6H_6N_6O_6$ ):TNT, detonation velocity 8.7 mm/microsecond). Initiation was provided by a RP-80 detonator (5). Total weight of the PWG was approximately 510 grams. A photograph of the PWG, with a test section of TNT attached to accept the shock wave, is shown in figure 2.

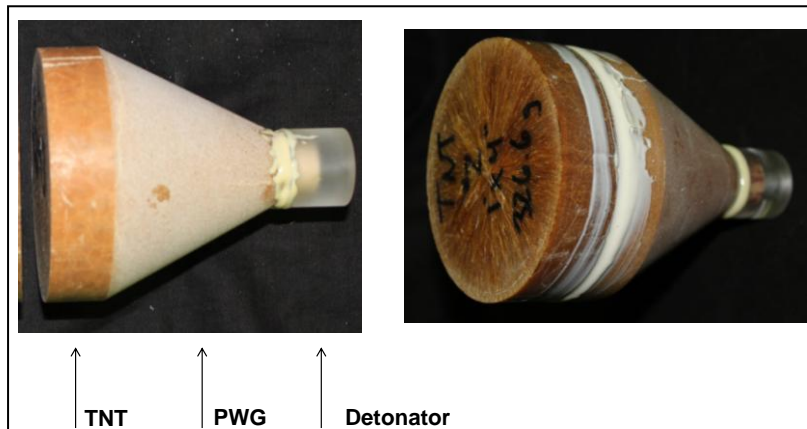


Figure 2. ARL explosive PWG with TNT test material.

Digital color images of the PWG face during function were obtained using a Cordin Company Model 570 Digital Framing Camera. This camera uses a rotating mirror assembly to sequentially expose 74 digital color cameras arranged in an arc about the mirror. The camera was operated at its maximum speed of 2.5 million frames per second. Exposure time per frame was 300 ns. Image resolution was 4 megapixels per frame. A 30 cm wide square mirror was used to reflect light emitted from the face of the PWG to the framing camera. The framing camera was equipped with a Nikon 70-300 telephoto lens at full aperture. A photograph of the Cordin Company Model 570 framing camera is shown in figure 3.



Figure 3. The Cordin Company Model 570 digital color framing camera.

---

### 3. Digital Color Imaging

---

Most color cameras employ a Bayer-type mask to generate color images. The Bayer-type mask generates sub-pixel output in red, green, and blue spectral regions for each frame recorded by the camera. For work reported here, a MATLAB program generates the three separate pixel arrays from each frame, enabling color-band specific digital image processing. To enable quantitative comparison of light output over the three filter bandwidths, each camera must go through a tedious calibration to map out the pixel response across the full visible spectrum (6). Camera calibration involves comparing sub-pixel output with the output from a calibrated photomultiplier tube for narrow bandwidth radiation over the full visible spectrum. Figure 4 shows a schematic of the Bayer-type mask in front of the sensor element of a typical color camera (a), a calibration graph for a high speed digital camera (for example only, not for the

Cordin imager) (b), and a schematic of the three color matrices generated per frame (c). Because each color-specific matrix contains zero signal at pixels filtered for other colors, manufacturer-specific zero-filling firmware is used to create complete color matrices for each frame (6).

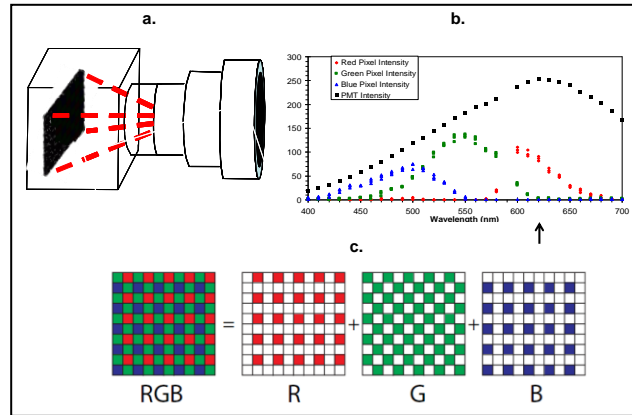


Figure 4. a. A schematic of the Bayer-type mask; b. A calibration spectrograph for the Bayer-type mask; and c. A schematic of deconvolution of a raw color image.

Figure 5a shows an image of a dispersed He:Ne laser beam, reflected by a sheet of paper, at a wavelength of 635 nanometers, obtained using the Cordin Model 570 camera. Figure 5b shows the red pixel matrix for this image. Figures 5c and 5d show the green and blue pixel matrices, respectively. Although the image appears predominantly in the red pixel matrix, careful examination shows some response in the green matrix. Note: The small arrow in figure 4b shows the wavelength position of the He:Ne laser on a Bayer-type calibration spectrograph.

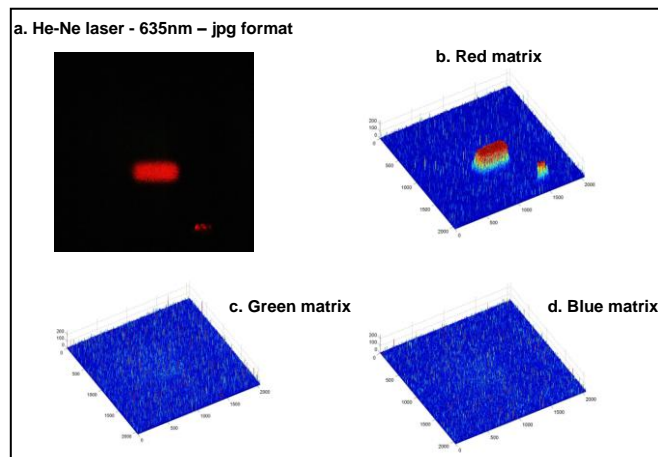


Figure 5. a. A color image of a dispersed, reflected He:Ne laser near a wavelength of 635 nm; b. The red matrix corresponding to a; c. The green matrix corresponding to a. (note some response) and d. The blue matrix corresponding to a.

---

## 4. Results

---

Figure 6 shows a series of color images of the PWG face following initiation. A glass cover slide was glued to the surface of the PWG to confine a small air gap (see figure 3 b). Shock-induced light emission from this air gap was used to determine time of shock wave arrival at the PWG surface (denoted as time  $t_0$ ). The dark stripe in the image in figure 6,  $t_0 + 400$  ns, is caused by the glass cover slide becoming non-transparent after shock wave passage.

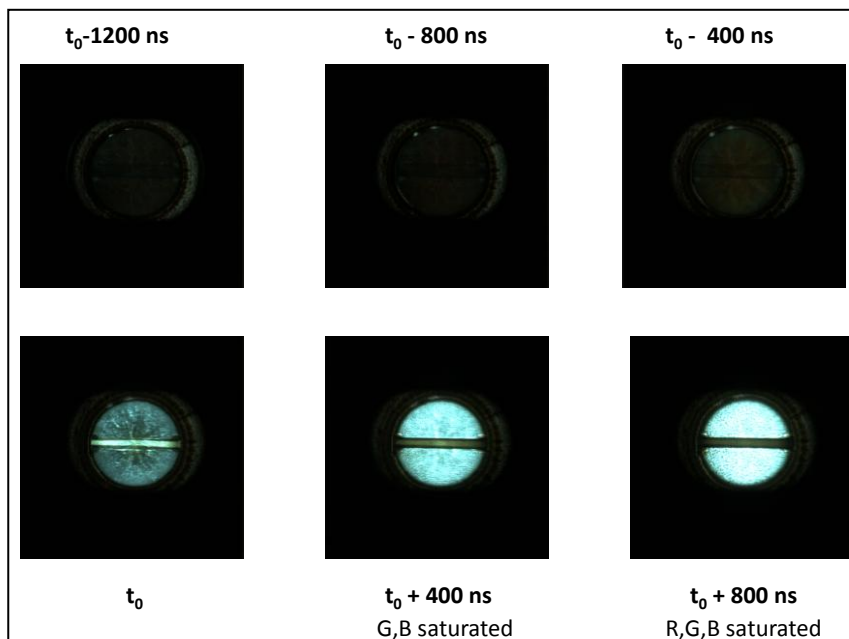


Figure 6. A series of images of light emission from the face of the PWG following initiation. The frame denoted as  $t_0$  corresponds to arrival of the shock wave at the PWG face. R,G,B refer to pixel color matrices (red, green, blue) used by the camera to produce color images.

Figure 7 shows contour maps of red matrices from images up to shock wave emergence (denoted as  $t_0$ ) at the face of the PWG, in time increments (400 ns) corresponding to the maximum speed of the camera. Since the exposure time of the camera is 300 ns per frame, each matrix in figure 7 corresponds to an integration of light over that period.

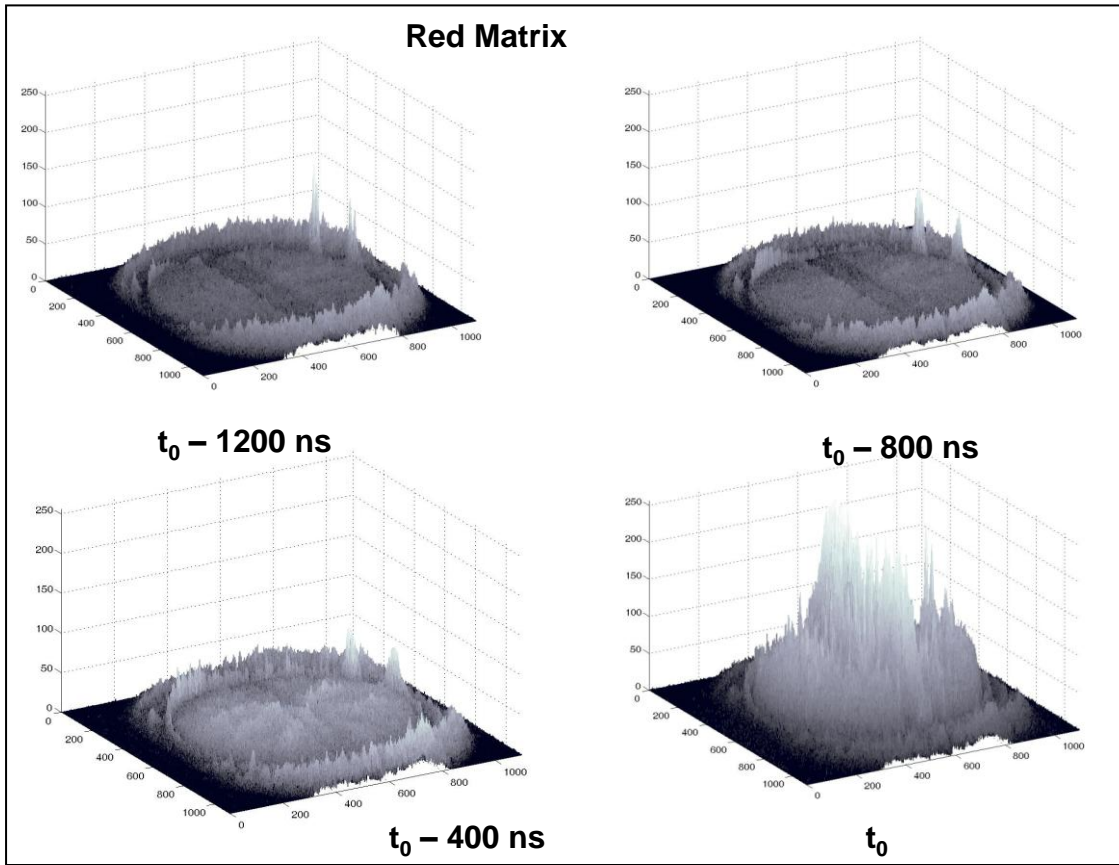


Figure 7. Contour maps of red matrices up to the time of the shock wave emerging from the face of the PWG.

Note: The intense band in the matrix for time  $t_0$  is caused by light emission from the small air gap between the glass cover slide and the face of the PWG. In each map, the vertical Z axis corresponds to light intensity, and the horizontal axes correspond to image pixel number.

Figure 8 shows contour maps of cross sections through the three sets of color matrices corresponding to light emission from the face of the PWG. The cross section is measured through the center of the image, 1 pixel wide, perpendicular to the long axis of the glass cover slide. In each cross sectional contour map, the horizontal x-axis denotes frame number, the y-axis denotes pixel number within the cross section (1 pixel wide), and the vertical axis is light intensity. In each contour map, the shockwave reaches the surface of the PWG at frame 19.

This is evident by the spike in intensity near cross section center at frame 19 in each contour map. Following passage of the shock through the glass cover slide, there is a sharp drop in intensity at cross section center caused by a loss in transparency of the glass. Each cross section also shows that there is significant light emission from within the PWG prior to shock wave emergence. For the three color matrices, the red matrix is last to saturate following shock emergence.

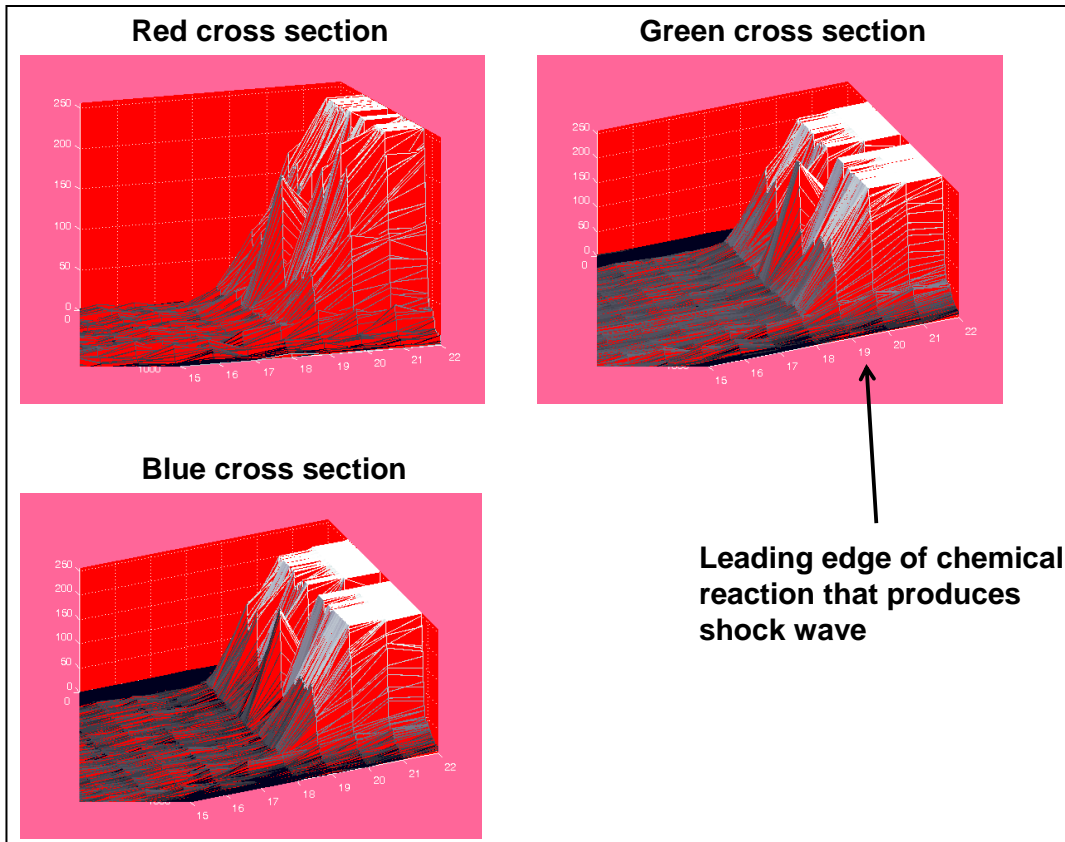


Figure 8. Cross sectional contour maps of the three color matrices.

Note: In each cross sectional contour map, the horizontal x-axis denotes frame number, the y-axis denotes pixel number within the cross section (1 pixel wide), and the vertical axis is light intensity. In each contour map, the shockwave reaches the surface of the PWG at frame 19. For the three color matrices, the red matrix is last to saturate following shock wave emergence.

---

## 5. Discussion

---

Figure 9 shows a detailed side view contour map of the red matrix cross section shown in figure 8. In this figure, the horizontal x-axis denotes frame number, the y-axis (into the plane of the page) denotes pixel number within the cross section (1 pixel wide), and the vertical axis is light intensity. The shock wave reaches the PWG surface at frame 19, denoted  $t_0$ . Figure 9 shows that there is appreciable light intensity in the red pixel matrices before and after the shock wave reaches the surface of the PWG.

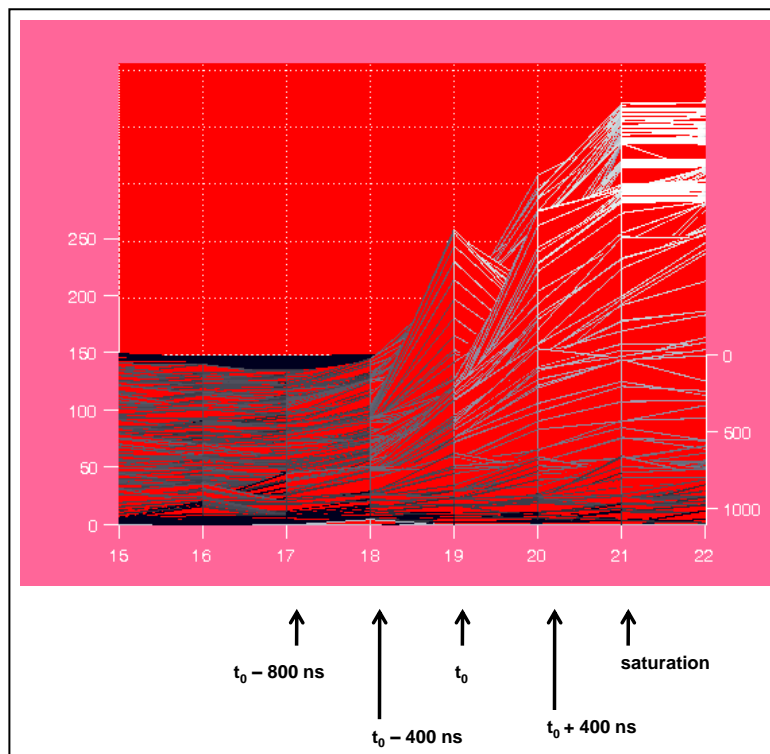


Figure 9: Side view of a contour map of red matrix cross sections near the time when the shock wave emerges from the face of the PWL.

Note: The horizontal x-axis denotes frame number, the y-axis (into the plane of the page) denotes pixel number within the cross section (1 pixel wide), and the vertical axis is light intensity. The shock wave reaches the PWG surface at frame 19, denoted  $t_0$ .

Figure 10 shows a series of 2-dimensional graphs of single cross sections through the red matrices viewed perpendicular to the long axis of the glass cover slide. In this figure, the horizontal x-axis corresponds to pixel number, and the vertical y-axis corresponds to single pixel intensity through the PWG surface centerline. Prior to shock wave emergence at the cross section corresponding to  $t_0$ , the profile of light emission intensity with pixel number appears to indicate a planar shock front in the material interior. At shock emergence, the profile of light emission intensity with pixel number appears much less linear. As a comparison, figure 11 shows a CTH simulation of shock transit in the ARL PWG (4). The CTH simulation predicts the PWG to produce a planar shock at most times following initiation (7).

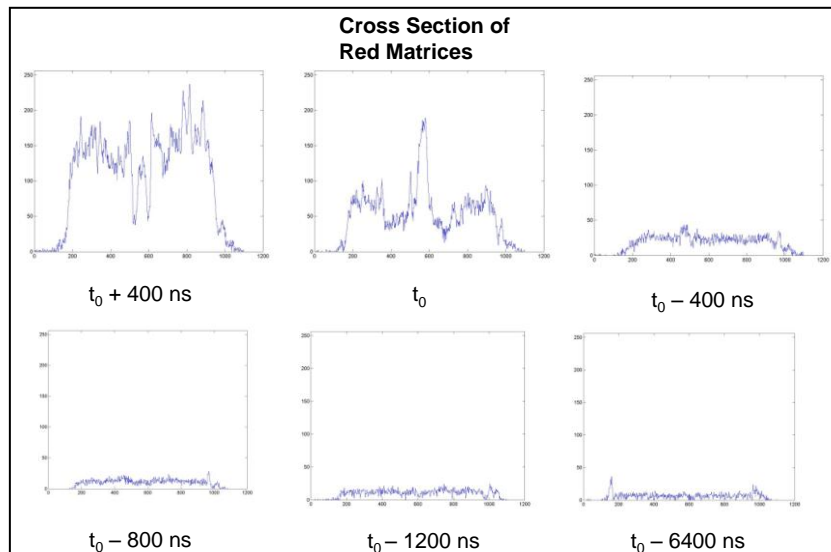


Figure 10. A series of 2-dimensional graphs of single cross sections through the red matrices viewed perpendicular to the long axis of the glass cover slide.

Note: The horizontal x-axis corresponds to pixel number, and the vertical y-axis corresponds to single pixel intensity through the PWG surface centerline.

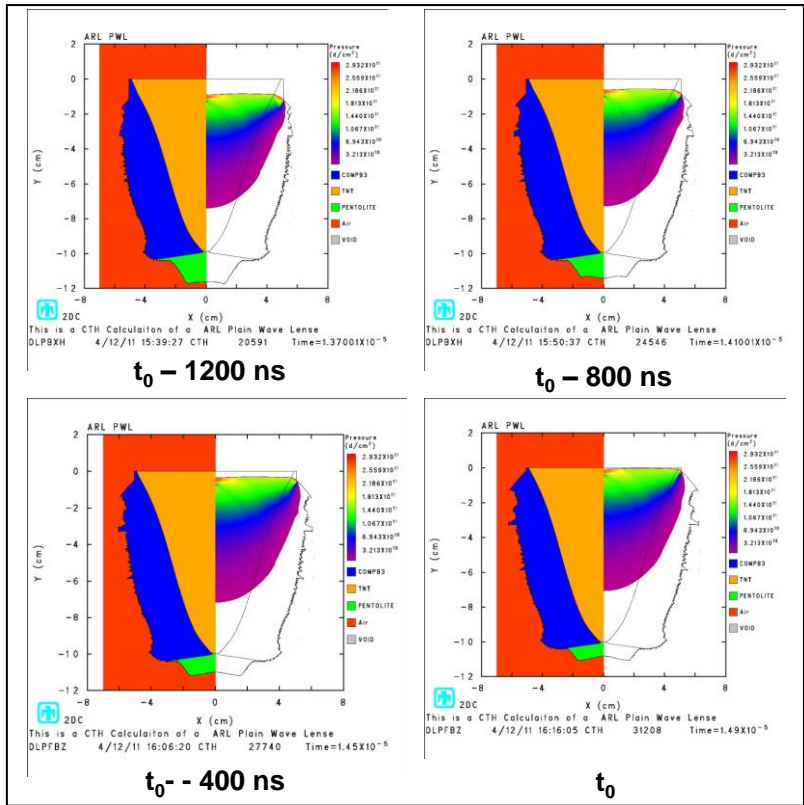


Figure 11. CTH simulations of shock wave transit in the ARL PWG.

Note: The right side of each figure corresponds pressure; the left side corresponds to detonation product gas distribution. The simulations predict a reasonably planar shock front at times near shock wave emergence from the face of the PWG.

The data suggest that using digital color imaging in a way similar to that shown here is a reasonable method of determining shock wave planarity within a solid explosive. The data also suggest that high speed digital imaging can provide quantitative information on explosive performance and chemistry. Because light emission at different wavelengths can be quantified as described above, temperatures at the explosive surface can be calculated. This has been done by us recently for outdoor explosions to predict influence of explosive casings on performance (6). Additionally, the data indicates that light being emitted from within the detonating material, prior to surface arrival of the detonation front, may be measured. We believe that this light is likely most influenced by incandescence from hot interior detonation products, but this light also includes that emitted by the detonation front within the explosive. An attempt to differentiate that light emission from the detonation product incandescence is beyond the present scope of this work.

---

## 6. Conclusions

---

Digital images of light emission from the face of an explosive PWG have been measured, and analyzed for intensity in each color matrix populated by a Cordin Company Model 570 digital framing camera. Light emission was measured before and after emergence of the shock wave from the face of the PWG. By using the known camera framing rate and the detonation velocity of the explosives in the PWG, it is estimated that there is measurable light intensity to a depth of at least 10 mm in TNT. At this depth, the measured light intensity appears relatively constant, correlating with simulation. However, it should be noted that the light reaching the camera from this depth is scattered by its passage through unreacted material. The nature of light reaching the camera prior to shock wave emergence from the face of the PWG is intriguing in that it should have at least a partial component emanating from the reaction zone. Estimation of planarity off the shock wave as it emerges from the PWG seems feasible, but a faster camera utilizing an intensified imager is recommended.

---

## 7. References

---

1. Weirick, L. J. *Plane Shock Generator Explosive Lens: Shock Characterization of 4340 and PH13-8Mo Steels, C360 Brass and PZT 65/35 Ferro-Electric Ceramic*; SAND93-3919 UC-742; Sandia National Laboratories: Albuquerque, New Mexico and Livermore, California, 1994.
2. Fritz, J. N. *A Simple Plane Wave Explosive Lens*; LA-11956-MS, UC-706 and UC-741; Los Alamos National Laboratory: Los Alamos, NM, 1990.
3. Benedick, W. B. Nitroguanidine Explosive Plane-Wave Generator for Producing Low Amplitude Shock Waves. *Rev. Sci. Instrum* **1965**, 36 (9), 1309-1315.
4. Kerley, G. I. *CTH Equation of State Package: Porosity and Reactive Burn Models*; SAND92-0553; Sandia National Laboratories: Albuquerque, NM, 1992.
5. Cooper, P. *Explosives Engineering*; Wiley-VCH: New York, 1996.
6. Densmore, John M.; Homan, Barrie E.; Biss, Matthew M.; McNesby, Kevin L. High-Speed Two-Camera Imaging Pyrometer for Mapping Fireball Temperatures, *Appl. Opt.* **2011**, 50 (33) 6267-6271.
7. Mader, C. L. *Numerical Modeling of Explosives and Propellants*, 3rd ed.; CRC Press: Boca Raton FL 2008.

1  
PDF DEFENSE TECH INFO CTR  
ATTN DTIC OCA  
8725 JOHN J KINGMAN RD STE 0944  
FT BELVOIR VA 22060-6218

3 US ARMY RSRCH LAB  
ATTN RDRL WML C G SUTHERLAND  
ATTN RDRL WML C R BENJAMIN  
ATTN RDRL WML C K L MCNESBY  
BLDG 1185  
APG MD 21005-5066

3 US ARMY RSRCH LAB  
ATTN IMAL HRA MAIL & RECORDS MGMT  
ATTN RDRL CIO LL TECHL LIB  
ATTN RDRL CIO LT TECHL PUB  
ADELPHI MD 20783-1197

INTENTIONALLY LEFT BLANK.